PREDICTION OF THE SPINDLE AND TOOL RECEPTANCE: INDUSTRIAL APPLICATION IN REAMING PROCESS

Jaouher SELMI[1,3*], Jean Philippe COSTES[1], Philippe LORONG[2], Gérard POULACHON[1], Patrice CARRAS[3]

[1]Arts et Métiers Paristech, LaBoMaP, Rue porte de Paris, Cluny, France

[2]Arts et Métiers Paristech, PIMM, Boulevard de l'hôpital, Paris, France

[3]RENAULT, Rue des bons raisins, Rueil Malmaison, France

* Corresponding author e-mail: jaouher.selmi@renault.com

Abstract

It is proposed to apply a methodology in order to evaluate the ability of different machining systems (Spindle/Tool) to run a reaming process in a stable way.The methodology is based on an experimental measurement of the dynamic behavior for the system including the spindle and the tool holder. Then, by coupling frequencies response functions, a new system (Spindle/Tool) FRF is predicted at the tool tip. Finally, the critical depth of cut is analytically calculated from the eigenvalues of the characteristic equation of the dynamic reaming process.

Keywords:

Spindle, Dynamic, Chatter, Stability, Reaming, FRF coupling

1 INTRODUCTION

Besides of machining-center power and torque limits, self-excited vibrations occurrence (chatter) constitutes a real productivity limitation. Peklenik and Gartner [Peklenik 1967], Pruvot [Pruvot 1995] and Koppka [Koppka 2008] have shown that stiffness lack in machining systems can have a negative effect on dimensional produced work piece accuracy.

Tlusty [Tlusty 1954] and Tobias [Tobias 1965] exposed the theory of regeneration; they demonstrated that the instability is due to this phenomenon and appears when a depth of cut threshold is reached. Besides, Altintas and Budak [Altintas 1995] have set a model for stability chart prediction in milling process. The lobe stability diagram is a chart which represents stability and instability domains during machining and allows the choice of preferential cutting conditions in order to increase productivity and avoid vibration. Thus, machining center reliability from avoiding chatter point of view depends on how machining center will be used.

Many other studies have been carried on spindle characterization, Gurney [Gurney 1961] , Sadek [Sadek 1970] and Yuce [Yuce 1983] have used the coefficient of Merit to compare spindles dynamic behavior by setting the structure into forced vibrations. In addition, Tobias [Tobias 1962] used stability chart as a comparative dynamic test certificate. Gagnol [Gagnol 2006] has performed studies on spindle dynamic behavior. Otherwise, Ertürk and Özsahin [Erturk 2006a], [Erturk 2006b] and [Ozsahin 2009] have performed studies on the spindle and the tool dynamic behavior. The studies were based on spindle FE model through beam receptance coupling. Besides, Wang [Wang 1996] has performed a study on spindle design improvement in order to avoid chatter in milling. He compared two different spindles design using different tools in the same cutting conditions. The used criterion was the depth of cut when chatter appears. Catania [Catania 2011] has used an approach based on the modal parameters identification in order to model the spindle and the frame of the machine tool. The tool was represented by a discrete modal approach. The semi-discretization method was used to fit the stability chart. Finally Namazi [Namazi 2007], has led a study on tool FRF prediction especially applied for shrink fit tooling.

The present paper does not focus on the spindle model establishment as it was done by Gagnol and Erturk. The spindle dynamic behavior is identified experimentally using a reference tool. Then, using receptance coupling ([Erturk 2006a], [Namazi 2007]), the FRF at the new tool tip is built.Then referring to the analatycal stability model in milling and drilling [Altintas 1995] and [Jochem 2007], it was considered that the reaming has the same behavior as drilling from lateral chatter point of view. In this way, the equations of stability model were adapted to be used with different reamer gemotries. In order to estimate critical stability limits [Tobias 1962] , the stability charts were fitted using the predicted dynamic properties at the tool tip and the cutting forces factors. The critical depth of cut in reaming process is used in the evaluation of the dynamic behavior of the machining system.

2 SPINDLE FRF MATRIX IDENTIFICATION:

2.1 Principle and definitions:

Three mechanical systems are introduced (Fig. 2). The used vocabulary will be defined as follows:

- $ystem_1$: The spindle, the tool holder and the forward section of the tool
- $ystem_2$: The spindle and the tool holder
- $ystem_3$: The forward section of the tool

Fig. 1: The reference tool

Note that the $System_2$ and the $System_3$ are linked through the rigid cross section illustrated in Fig. 2.

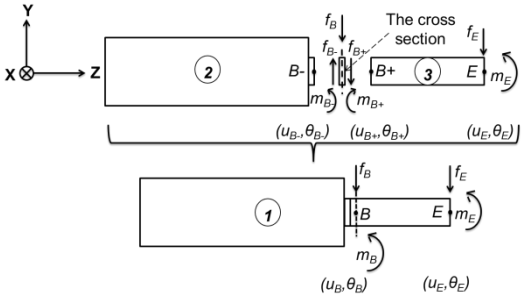

Fig. 2: The $ystem_1$, the $ystem_2$ and the $ystem_3$

The aim of this subsection is to show a general methodology applicable for all kind of machine tool in order to identify the $System_2$ FRF matrix at B- (Fig. 4). The principle is based on measurements using a reference tool and calculations. All the study is made for a 2D problem supposing that the dynamic behavior of the spindle is axisymmetric. If it is not the case, this analysis must be conducted in two orthogonal planes parallel to Z axis of the spindle. Furthermore, the motion of the joint cross section (Fig. 2) between the $system_2$ and the $system_3$ is well characterized by transversal displacement on Y direction and rotation around X direction.

The use of the reference tool is useful for getting all the needed terms of the $System_2$ FRF matrix. This matrix will represent the whole dynamic behavior of the $System_2$ at B- taking into account its transversal displacement and bending rotation responses and will be defined later through the equation (6). Without this intermediate mean, the $system_2$ FRF matrix is hard to obtain directly by measurement. We notice that bending moments and rotations at the cross-section can not be measured with simple hammer test method. This trial gives results only about transversal forces and displacements. In this way, hammer shocks are conducted on the $System_1$ as depicted in the Fig. 3 and have as results the acquisition of the transfert functions $h^1_{EE,uu}$, $h^1_{BB,uu}$, $h^1_{EB,uu}$ which are defined as follows :

$$h^1_{EE,uu}\, f_E = u_E \tag{1}$$

$$h^1_{BB,uu}\, f_B = u_B \tag{2}$$

$$h^1_{EB,uu}\, f_E = u_B \quad or \quad h^1_{BE,uu}\, f_B = u_E \tag{3}$$

Where f_j and u_j are respectively the transversal force and displacement at the point $_j$. The obtained FRFs will be used in the presented approach which will drive to the identification of the entire FRF matrix of the $System_1$.

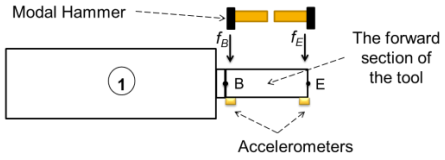

Fig. 3: The experimental configuration using the spindle and the reference tool

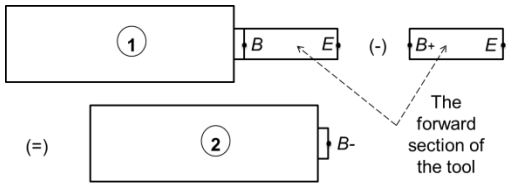

Fig. 4: The spindle identification approach

Besides, the vibrations are supposed to be led by the dynamic behavior of the spindle and the tool. Therefore, the machine tool frame influence on vibrations will be neglected. Note that *f* and *M* represent respectively, the shear force and the bending moment, and u and θ are the transversal displacement and bending rotation angle.

- (f_B, m_B): The external forces vector at B
- (f_{B-}, m_{B-}): The action at the cross section of the $system_2$ at B_-
- (f_{B+}, m_{B+}): The action at the cross section of the $system_3$ at B_+
- (f_E, m_E): The external forces vector at E

$\boldsymbol{H^1}$, $\boldsymbol{H^2}$ and $\boldsymbol{H^3}$ are respectively condensed FRF matrix of the systems $(1,2,3)$ presented in the Fig. 2, they are defined between the points E and B such as :

- $ystem_1$: The spindle and the reference Tool

$$\boldsymbol{H^1}\begin{pmatrix} f_B \\ m_B \\ f_E \\ m_E \end{pmatrix} = \begin{pmatrix} u_B \\ \theta_B \\ u_E \\ \theta_E \end{pmatrix} With, \boldsymbol{H^1} = \begin{pmatrix} \boldsymbol{H^1_{BB}} & \boldsymbol{H^1_{BE}} \\ \boldsymbol{H^1_{EB}} & \boldsymbol{H^1_{EE}} \end{pmatrix} \tag{4}$$

$\boldsymbol{H^1}$ can be detailed as :

$$\begin{pmatrix} h^1_{BB,uu} & h^1_{BB,u\theta} & h^1_{BE,uu} & h^1_{BE,u\theta} \\ h^1_{BB,\theta u} & h^1_{BB,\theta\theta} & h^1_{BE,\theta u} & h^1_{BE,\theta\theta} \\ h^1_{EB,uu} & h^1_{EB,u\theta} & h^1_{EE,uu} & h^1_{EE,u\theta} \\ h^1_{EB,\theta u} & h^1_{EB,\theta\theta} & h^1_{EE,\theta u} & h^1_{EE,\theta\theta} \end{pmatrix} \begin{pmatrix} f_B \\ m_B \\ f_E \\ m_E \end{pmatrix} = \begin{pmatrix} u_B \\ \theta_B \\ u_E \\ \theta_E \end{pmatrix} \tag{5}$$

- $ystem_2$: The spindle and the tool holder

$$\boldsymbol{H^2_{BB}}\begin{pmatrix} f_{B-} \\ m_{B-} \end{pmatrix} = \begin{pmatrix} u_{B-} \\ \theta_{B-} \end{pmatrix} \tag{6}$$

Is equivalent to :

$$\begin{pmatrix} h^2_{BB,uu} & h^2_{BB,u\theta} \\ h^2_{BB,\theta u} & h^2_{BB,\theta\theta} \end{pmatrix} \begin{pmatrix} f_{B-} \\ m_{B-} \end{pmatrix} = \begin{pmatrix} u_{B-} \\ \theta_{B-} \end{pmatrix} \quad (7)$$

- $ystem_3$: The forward section of the tool

$$\boldsymbol{H^3} \begin{pmatrix} f_{B+} \\ m_{B+} \\ f_E \\ m_E \end{pmatrix} = \begin{pmatrix} u_{B+} \\ \theta_{B+} \\ u_E \\ \theta_E \end{pmatrix} With, \boldsymbol{H^3} = \begin{pmatrix} \boldsymbol{H^3_{BB}} & \boldsymbol{H^3_{BE}} \\ \boldsymbol{H^3_{EB}} & \boldsymbol{H^3_{EE}} \end{pmatrix} \quad (8)$$

Then

$$\begin{pmatrix} h^3_{BB,uu} & h^3_{BB,u\theta} & h^3_{BE,uu} & h^3_{BE,u\theta} \\ h^3_{BB,\theta u} & h^3_{BB,\theta\theta} & h^3_{BE,\theta u} & h^3_{BE,\theta\theta} \\ h^3_{EB,uu} & h^3_{EB,u\theta} & h^3_{EE,uu} & h^3_{EE,u\theta} \\ h^3_{EB,\theta u} & h^3_{EB,\theta\theta} & h^3_{EE,\theta u} & h^3_{EE,\theta\theta} \end{pmatrix} \begin{pmatrix} f_{B+} \\ m_{B+} \\ f_E \\ m_E \end{pmatrix} = \begin{pmatrix} u_{B+} \\ \theta_{B+} \\ u_E \\ \theta_E \end{pmatrix} \quad (9)$$

2.2 The FE definition of the tool:

The reference tool is composed of the tool holder and the forward section of the tool (Fig.4) which is characterized by a given diameter, length, density ρ (Kg/m^3) and Young modulus E (GPa). The tools are represented by a finite elements models. The equation of motion on their nodes can be written as follows :

$$\mathbf{K}\,\boldsymbol{q} + \mathbf{M}\,\ddot{\boldsymbol{q}} = \boldsymbol{f} \quad (10)$$

Where, $\boldsymbol{K}$ and $\boldsymbol{M}$ are respectively the stiffness and mass matrix of the FE model, and $\boldsymbol{f}$ and $\boldsymbol{q}$ are the generelized vectors of force and displacement. Assuming an harmonic response solution of the equation (10) :

$$\boldsymbol{q} = \mathbf{q}\, e^{j\omega t} \text{ and } \boldsymbol{f} = \mathbf{f}\, e^{j\omega t} \quad (11)$$

Using the equations (10) and (11) drives to :

$$(\mathbf{K} - \omega^2\mathbf{M})^{-1}\mathbf{f} = \mathbf{q} \quad (12)$$

The FRF matrix $\boldsymbol{H^3}$ of the tool can be written as follows:

$$\boldsymbol{H^3} = (\mathbf{K} - \omega^2\mathbf{M})^{-1} \quad (13)$$

It is considered that the structural damping of the tool is neglected comparing to the spindle damping.

2.3 Experimental method/model entries:

All of the presented tests in this section were made on the same machining center (DMG). The machine center used is a three axes architecture, equipped with a spindle (KESSLER) and ball screw axis technology. The spindle can be moved in the working space following the three directions (X, Y and Z). Impulse hammer shocks are conducted on the reference tool at the points B and E in order to obtain 3 FRF (h^1_{EE} , h^1_{BB}, and $h^1_{EB} = h^1_{BE}$) which are required to identify the $ystem_2$ dynamic behavior through the matrix $\boldsymbol{H^2_{BB}}$ defined in the equation (6). The experimental setup is depicted in the Fig. 3. Hammer tests were made following the instructions and the details described below:

- Two low mass bandwidth accelerometers [Sensitivity: 100mV/g] were located on the reference tool like depicted in (Fig. 3) and connected to a computer through 50 kHz frequency data acquisition card.
- A modal hammer [Sensitivity: 2,27mV/N] was connected to the acquisition card.

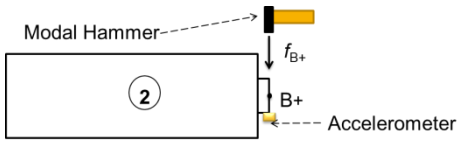

Fig. 5: The experimental configuration using the spindle and the tool holder

Besides, other experimental tasks are performed on the $ystem_2$ as depicted in the Fig. 5. Then, the used equipement and configurations are the same as used before. In this experimental task, the transversal FRF at the point B- is generated. It will be compared in the next paragraph with the calculated results. This step has been done for verification and only for the transversal FRF of the $ystem_2$. However, the other components of the matrix $\boldsymbol{H^2_{BB}}$ are difficult to obtain directly by measurement and are established only by calculations.

2.4 The identified dynamic behavior of the $\mathbf{System_2}$:

The objective of this subsection is to show the identified FRFs of the matrix $\boldsymbol{H^2_{BB}}$. Those functions will be used later in order to predict the dynamic behavior at the tool tip. Knowing that $\boldsymbol{H^2_{BB}}$ is symmetric. It contains 3 FRF and can be expressed such as :

$$\boldsymbol{H^2_{BB}} = \begin{pmatrix} h^2_{BB,uu} & h^2_{BB,u\theta} \\ h^2_{BB,\theta u} & h^2_{BB,\theta\theta} \end{pmatrix} \quad (14)$$

The resolution of the equations (1), (2), (3), (5), (7), (9), (21) and (22) drives to the identification of the transfert functions which constitute the matrix $\boldsymbol{H^2_{BB}}$ of the $system_2$: $h^2_{BB,uu}$, $h^2_{BB,\theta\theta}$, $h^2_{BB,u\theta}$ and $h^2_{BB,\theta u}$. These functions are illustrated in the Fig. 6 and Fig. 7.

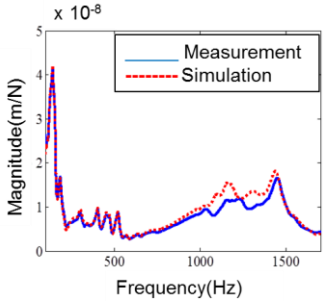

Fig. 6: The measured and the calculated transversal FRF $h^2_{BB,uu}$ of the $ystem_2$

The Fig. 6 shows results of the modeled and the experimentally measured FRF at the point B of the

$System_2$. The accuracy of the depicted results (Fig. 6) makes the approach reliable. It has been noted that the measurement of the FRFs of the bending rotations is difficult. Then, the other component of the matrix $\boldsymbol{H^2_{BB}}$ can be predicted only by simulation (Fig. 7). This application was made using a solid tool with high stiffness and high first natural frequency in order to minimize the disturbance related to the tool in the studied frequencies range. The same approach can be applied on different kind of spindle with different tool holder technologies. Thus, the spindles dynamic properties can constitute a data base for machining process design activities.

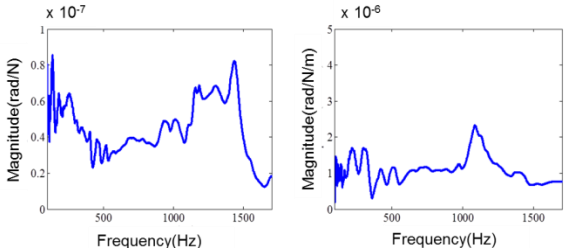

Fig. 7: The calculated $h^2_{BB,u\theta}$ and $h^2_{BB,\theta\theta}$ of the $System_2$

3 THE PREDICTION OF THE NEW TOOL TIP FRF:

3.1 The FRFs coupling model:

In the present subsection, a FRF coupling methodology based on results obtained previously will be shown.

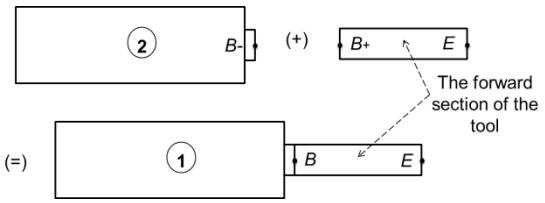

Fig. 8: The FRF at the tool tip prediction approach

The objective is to obtain the new tool tip matrix $\boldsymbol{H^1_{EE}}$ (16) using the reached results. Its transversal component $h^1_{EE,uu}$ will be used later for stability lobes establishment in reaming process. Different kind of models can be used in order to represent the dynamic behavior of the tool, among others, analytical model or full 3D FE model. For the shown results, a 2D FE model was used. The principle of this approach consists in representing the $system_1$ by a dynamic model at the tool tip. This result can be obtained through coupling the $system_2$ and the $system_3$ FRF matrix. Therefore, all of the transfert functions $h^2_{BB,uu}$, $h^2_{BB,u\theta}$ and $h^2_{BB,\theta\theta}$ of the matrix $\boldsymbol{H^2_{BB}}$ are required. It will be supposed that tool active parts (rakes parts of the teeths) have a rigid motion. In the following developments we use the definitions below:

• $System_1$:

$$\boldsymbol{H^1}\begin{pmatrix} f_B \\ m_B \\ f_E \\ m_E \end{pmatrix} = \begin{pmatrix} u_B \\ \theta_B \\ u_E \\ \theta_E \end{pmatrix} \text{With, } \boldsymbol{H^1} = \begin{pmatrix} \boldsymbol{H^1_{BB}} & \boldsymbol{H^1_{BE}} \\ \boldsymbol{H^1_{EB}} & \boldsymbol{H^1_{EE}} \end{pmatrix} \quad (15)$$

Considering that external forces are equal to zero at B, the relation between the displacements and forces at E is the following:

$$\boldsymbol{H^1_{EE}}\begin{pmatrix} f_E \\ m_E \end{pmatrix} = \begin{pmatrix} u_E \\ \theta_E \end{pmatrix} \quad (16)$$

• $System_2$:

$$\boldsymbol{H^2_{BB}}\begin{pmatrix} f_{B-} \\ m_{B-} \end{pmatrix} = \begin{pmatrix} u_{B-} \\ \theta_{B-} \end{pmatrix} \quad (17)$$

• $System_3$:

$$\boldsymbol{H^3}\begin{pmatrix} f_{B+} \\ m_{B+} \\ f_E \\ m_E \end{pmatrix} = \begin{pmatrix} u_{B+} \\ \theta_{B+} \\ u_E \\ \theta_E \end{pmatrix} \text{ with } \boldsymbol{H^3} = \begin{pmatrix} \boldsymbol{H^3_{BB}} & \boldsymbol{H^3_{BE}} \\ \boldsymbol{H^3_{EB}} & \boldsymbol{H^3_{EE}} \end{pmatrix} \quad (18)$$

then,

$$\boldsymbol{H^3_{BB}}\begin{pmatrix} f_{B+} \\ m_{B+} \end{pmatrix} + \boldsymbol{H^3_{BE}}\begin{pmatrix} f_E \\ m_E \end{pmatrix} = \begin{pmatrix} u_{B+} \\ \theta_{B+} \end{pmatrix} \quad (19)$$

and,

$$\boldsymbol{H^3_{EB}}\begin{pmatrix} f_{B+} \\ m_{B+} \end{pmatrix} + \boldsymbol{H^3_{EE}}\begin{pmatrix} f_E \\ m_E \end{pmatrix} = \begin{pmatrix} u_E \\ \theta_E \end{pmatrix} \quad (20)$$

Coupling the $systems_2$ and the $system_3$ FRF matrix is made through the joint cross section forces equilibrium and motion continuity. The vectors expressions are written respectively like below, considering that no external forces are applied on both the $systems_2$ and the $system_3$:

$$\begin{pmatrix} f_{B+} \\ m_{B+} \end{pmatrix} + \begin{pmatrix} f_{B-} \\ m_{B-} \end{pmatrix} = \begin{pmatrix} 0 \\ 0 \end{pmatrix} \quad (21)$$

and,

$$\begin{pmatrix} u_B \\ \theta_B \end{pmatrix} = \begin{pmatrix} u_{B+} \\ \theta_{B+} \end{pmatrix} = \begin{pmatrix} u_{B-} \\ \theta_{B-} \end{pmatrix} \quad (22)$$

Through the resolution of the equations system (16, 17, 19, 20, 21 and 22), the FRF matrix of the whole $system_1$ at the tool tip can be expressed as:

$$\boldsymbol{H^1_{EE}} = \boldsymbol{H^3_{EE}} - \boldsymbol{H^3_{BE}}(\boldsymbol{H^2_{BB}} + \boldsymbol{H^3_{BB}})^{-1}\boldsymbol{H^3_{EB}} \quad (23)$$

The equation (23) uses the matrix $\boldsymbol{H^2_{BB}}$ with the identified functions in the subsection (2.4) to constitute the FRF at the tool tip.

3.2 Experimental validation:

Impulse hammer shocks were performed at the reaming tools tip in order to get the transversal FRF $h^1_{EE,uu}$. The measurement configuration is depicted in Fig. 9. Besides, tasks were performed at the same conditions as presented in the subsection (2.3). The used tools have the characteristics detailed in the table 1.

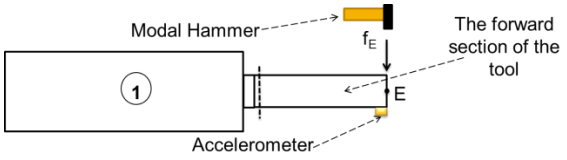

Fig. 9: The experimental configuration using the spindle and the tool

Tab. 1: The tools properties

	$Tool_1$	$Tool_2$
E (GPa)	195	210
$\rho(Kg/m3)$	7600	7600
Diameter (mm)	31	40
Length (mm)	143	223
Teeth number	3	3

3.3 Results and discussions:

The graphs depicted in the Fig. 10 are the representation of the modeled FRF as compared with measured one. Both of them are illustrated at the tool tip. The closeness of the experimentally measured and modeled FRF shows a good correlation. In a high speed spindle using ball bearing guiding outfit, its static stiffness is a speed dependent because of the gyroscopic effect and centrifugal forces action on the balls ([Gagnol 2011] and [Abele 2004]). Also, the dynamic properties of the spindle changes and can be seen regarding the tool tip [Abele 2010] . However, centrifugal forces and gyroscopic effects start to have a weight only at high speeds, at lower speeds these effect could be neglected. This study focuses on the reaming process of cast iron where the rotation speed remain inferior to 2000 rpm for the studied tools.

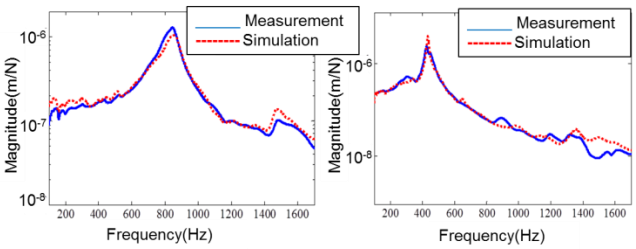

Fig. 10: The measured and calculated FRF at the $tool_1$ tip (on the left) and the $tool_2$ tip (on the right)

Otherwise, the identified FRFs of the $System_2$ were made at a given position of the workspace. As it was noted that the dynamic behavior was a spindle position dependent, the obtained results are valid only around the studied one. Nevertheless, the same method can be applied at particular positions of the work space in order to get the whole representation of dynamic properties of the studied machine. If we want to make the full study, its complexity depends on the number of degree of freedom of the spindle. For example, in automative industry, spindles are often horizontal and equipped only by X and Y translation axis.

4 APPLICATION IN THE REAMING PROCESS:

The objective of this subsection is to show how to compare different machining systems using the methodology described before. The principle is based on fitting the stability lobes through the predicted FRF for a known tool geometry and mechanical parameters.

The evaluation of machining system is based on the critical depth of cut criterion ap_{cri}. It is defined as the maximum depth of cut which is stable at ***all*** speeds. Above this depth of cut chatter can arise in certain speed bands which are separated from each others by chatter free speed bands [Tobias 1962].

4.1 Analytical prediction of chatter vibration in reaming

Roukema and Altintas have presented an analytical prediction of the stability lobes in drilling process [Jochem 2007], taking into account the chip thickness, and the cutting forces variation during machining. Considering that the drilling and the reaming have the same behavior from lateral vibrations point of view, a model for three flutes reamer is presented.

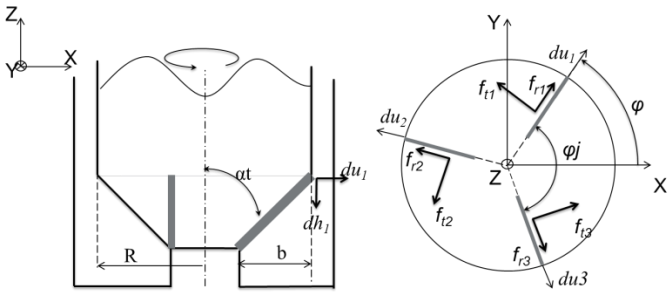

Fig. 11: The reaming model principle

It is supposed that forces are proportional to the chip area. Then, the forces on each flute are defined as :

$$f_{t1} = k_t b(h_1 + dh_1), f_{r1} = k_r f_{t1} \quad (24)$$

$$f_{t2} = k_t b(h_2 + dh_2), F_{r2} = k_r f_{t2} \quad (25)$$

$$f_{t3} = k_t b(h_3 + dh_3), F_{r3} = k_r f_{t3} \quad (26)$$

Where f_{tj}, f_{rj}, k_t, k_r, b, h and dh are respectively the tangential and radial forces at the flute having the index j, the tangential and radial cutting factors, the width of cut, the static chip thickness and the dynamic chip thickness. The total force applied at the tool tip on X and Y directions:

$$f_x = -f_{t1}sin(\varphi) - f_{t2}sin(\varphi + \varphi_j) - f_{t3}sin(\varphi + 2\varphi_j) + f_{r1}cos(\varphi) + f_{r2}cos(\varphi + \varphi_j) + f_{r3}cos(\varphi + 2\varphi_j) \quad (27)$$

$$f_y = f_{t1}cos(\varphi) + f_{t2}cos(\varphi + \varphi_j) + f_{t3}cos(\varphi + 2\varphi_j) + f_{r1}sin(\varphi) + f_{r2}sin(\varphi + \varphi_j) + f_{r3}sin(\varphi + 2\varphi_j) \quad (28)$$

Where φ and φ_j are the rotation angle of the tool and the reamer pitch angle as illustrated in Fig.11.

4.1.1 Dynamic reaming model

Because of the regenerative displacement dx and dy at the tool tip, a variating chip thickness dh on each flute is produced. The radial generated displacement at each flute is presented in the Fig. 11 and can be expressed as :

$$du_1 = dx\,cos(\varphi) + dy\,sin(\varphi) \quad (29)$$

$$du_2 = dx\,cos(\varphi + \varphi_j) + dy\,sin(\varphi + \varphi_j) \quad (30)$$

$$du_3 = dx\,cos(\varphi + 2\varphi_j) + dy\,sin(\varphi + 2\varphi_j) \quad (31)$$

The chip thickness variation dh_i is related to the radial displacement through the tool tip angle α_t (Fig. 11) and can be written such as :

$$dh_1 = \frac{dx\,cos(\varphi)+dy\,sin(\varphi)}{tan(\alpha_t)} \quad (32)$$

$$dh_2 = \frac{dx\,cos(\varphi+\varphi_j)+dy\,sin(\varphi+\varphi_j)}{tan(\alpha_t)} \quad (33)$$

$$dh_3 = \frac{dx\,cos(\varphi+2\varphi_j)+dy\,sin(\varphi+2\varphi_j)}{tan(\alpha_t)} \quad (34)$$

Knowing that the static component of the chip thickness has no influence on the stability study, the dynamic forces will be expressed using the dynamic chip expressions. The use of (24), (25), (26), (27) and (28) drives to:

$$df_x = k_t b(-dh_1\sin(\varphi) - dh_2\sin(\varphi + \varphi_j) - dh_3 sin(\varphi + 2\varphi_j)) + k_t k_r b(dh_1 cos(\varphi) + dh_2 cos(\varphi + \varphi_j) + dh_3 cos(\varphi + 2\varphi_j)) \quad (35)$$

$$df_y = k_t b(dh_1\cos(\varphi) + dh_2\cos(\varphi + \varphi_j) + dh_3 cos(\varphi + 2\varphi_j)) \quad + k_t K_r b(dh_1 sin(\varphi) + dh_2 sin(\varphi + \varphi_j) + dh_3 sin(\varphi + 2\varphi_j)) \quad (36)$$

The equations (32), (33), (34), (35) and (36) drives to :

$$df_x = \frac{k_t b}{\tan(\alpha_t)}\{[-\cos(\varphi)\sin(\varphi) - \cos(\varphi + \varphi_j)\sin(\varphi + \varphi_j)) - \cos(+2\varphi_j)\sin(\varphi + 2\varphi_j)] + k_r[\cos(\varphi)^2 + \cos(\varphi + \varphi_j)^2 + cos(\varphi + 2\varphi_j)^2]\}dx + \frac{k_t b}{\tan(\alpha_t)}\{[-sin(\varphi)^2 - sin(\varphi + \varphi_j)^2 - sin(\varphi + 2\varphi_j)^2] + k_r\ [\cos(\varphi)\sin(\varphi) + \cos(\varphi + \varphi_j)\sin(\varphi + \varphi_j) + cos(\varphi + 2\varphi_j)sin(\varphi + 2\varphi_j)]\}dy \quad (37)$$

$$df_y = \frac{k_t b}{tan(\alpha_t)}\{[cos(\varphi)^2 + cos(\varphi + \varphi_j)^2 + cos(\varphi + 2\varphi_j)^2 + k_r(\cos(\varphi)\sin(\varphi) + \cos(\varphi + \varphi_j)\sin(\varphi + \varphi_j) + cos(\varphi + 2\varphi_j)sin(\varphi + 2\varphi_j)]\}dx + \frac{k_t b}{\tan(\alpha_t)}\{[sin(\varphi)cos(\varphi) + sin(\varphi + \varphi_j)cos(\varphi + \varphi_j) + sin(\varphi + 2\varphi_j)cos(\varphi + 2\varphi_j)] + k_r[sin(\varphi)^2 + sin(\varphi + \varphi_j)^2 + sin(\varphi + 2\varphi_j)^2]\}dy \quad (38)$$

Then, the time depending directional factors matrix $\boldsymbol{B(t)}$ can be defined as :

$$\boldsymbol{B(t)}\begin{pmatrix}dx\\dy\end{pmatrix} = k_t b\begin{pmatrix}b_{xx}(t) & b_{xy}(t)\\ b_{yx}(t) & b_{yy}(t)\end{pmatrix}\begin{pmatrix}dx\\dy\end{pmatrix} = \begin{pmatrix}df_x\\df_y\end{pmatrix} \quad (39)$$

This matrix is periodic and will be approximated by the average component of the Fourrier series as :

$$\mathbf{B_0} = \frac{1}{T}\int_0^T \boldsymbol{B(t)}dt \quad (40)$$

$\mathbf{B_0}$ is valid between the entry and exit angles φ_{st} and φ_{ex} which are 0 and $\frac{2\pi}{z}$, where z is the flute number which is equal to 3 for a 3 flutes reamer. It is defined as :

$$\mathbf{B_0} = \frac{z}{2\pi}k_t b\mathbf{B_{red}} = \frac{z}{2\pi}k_t b\begin{pmatrix}b_{xx} & b_{xy}\\ b_{yx} & b_{yy}\end{pmatrix} \quad (41)$$

Through the equations (37), (38), (39), (40) and (41), the different component of the matrix $\mathbf{B_{red}}$ can be written as :

$$b_{xx} = \frac{1}{\tan(\alpha_t)}\int_0^{\frac{2\pi}{3}}\{(-\cos(\varphi)\sin(\varphi) - \cos(\varphi + \varphi_j)\sin(\varphi + \varphi_j) - \cos(\varphi + 2\varphi_j)\sin(\varphi + 2\varphi_j))K_r(\cos(\varphi)^2 + \cos(\varphi + \varphi_j)^2 + \cos(\varphi + 2\varphi_j)^2))\} = \frac{\pi k_r}{\tan(\alpha_t)} \quad (42)$$

$$b_{xy} = -\frac{\pi k_r}{\tan(\alpha_t)} \quad (43)$$

$$b_{yx} = \frac{\pi k_r}{\tan(\alpha_t)} \quad (44)$$

$$b_{yy} = \frac{\pi k_r}{\tan(\alpha_t)} \quad (45)$$

Therefore :

$$\mathbf{B_0} = \frac{z}{2\pi}k_t b\begin{pmatrix}\frac{\pi k_r}{\tan(\alpha_t)} & -\frac{\pi k_r}{\tan(\alpha_t)}\\ \frac{\pi k_r}{\tan(\alpha_t)} & \frac{\pi k_r}{\tan(\alpha_t)}\end{pmatrix} \quad (46)$$

Then, considering that $\boldsymbol{\delta_r}$ is the displacement vector, the dynamic reaming force equation become :

$$\boldsymbol{f(t)} = \frac{z}{2\pi}K_t b\mathbf{B_{red}}\boldsymbol{\delta_r} \quad (47)$$

4.1.2 Frequency domain solution

The charecteristic equation of the reaming process was analitically solved referring to Altintas and Budak method [Altintas 1995]. Considering the transfert functions matrix at the tool tip $\boldsymbol{H}_{\boldsymbol{EE}}^{\mathbf{rad}}(i\omega_c)$, the harmonic regenerative displacement at the chatter frequency ω_c can be described in the frequency domain as:

$$\boldsymbol{\delta}(i\omega_c t) = \boldsymbol{r}(i\omega_c t) - \boldsymbol{r}(i\omega_c T) = \left[1 - e^{-i\omega_c T}\right] e^{-i\omega_c t} \boldsymbol{H}_{\boldsymbol{EE}}^{\mathbf{rad}} \boldsymbol{f}$$

with $$\boldsymbol{H}_{\boldsymbol{EE}}^{\mathbf{rad}} = \begin{pmatrix} h_{EE,uu}^{1} & 0 \\ 0 & h_{EE,uu}^{1} \end{pmatrix} \quad (48)$$

Where $\omega_c T$ is the phase delay between the vibrations at successive tooth period T.

$$\boldsymbol{f} e^{-i\omega_c t} = \frac{1}{2} \mathrm{bk_t} [1 - \mathrm{e}^{-\mathrm{i}\omega_c \mathrm{T}}] \mathbf{B}_{\mathbf{red}} \boldsymbol{H}_{\boldsymbol{EE}}^{\mathbf{rad}} \boldsymbol{f} \quad (49)$$

The characterestic equation of the reaming process has a non trivial solution if the determinant is equal to zero :

$$det[\mathbf{I} - \frac{1}{2} \mathrm{k_t b} (1 - e^{-i\omega_c T}) \mathbf{B}_{\mathbf{red}} \boldsymbol{H}_{\boldsymbol{EE}}^{\mathbf{rad}}] = 0 \quad (50)$$

The solution of this equation is found using the eigenvalues of the characterestic equation :

$$det[\mathbf{I} - \lambda \mathbf{B}_{\mathbf{red}} \boldsymbol{H}_{\boldsymbol{EE}}^{\mathbf{rad}}] = 0 \quad (51)$$

λ and κ are defined as follws :

$$\lambda = \frac{-\mathrm{z}}{4\pi} \mathrm{bk_t} (1 - e^{-i\omega_c T}) \quad (52)$$

$$\kappa = \frac{\lambda_I}{\lambda_R} = \frac{sin(\omega_c T)}{1 - cos(\omega_c T)} \quad (53)$$

Where λ_R and λ_I are the real and imaginary parts of λ. T and ω_c are respectively the tooth passing period and the chatter frequency. Therefore, the stability lobes are fitted using the following equations :

$$b_{lim} = \frac{-2\pi\lambda_R}{\mathrm{zK_t}} (1 + \kappa^2) \quad (54)$$

$$T = \frac{1}{\omega_c} (\varepsilon + 2k\pi) -> n = \frac{60}{z\,T} \quad (55)$$

Where n, ε and z are respectively the rotation speed in (rpm), the phase shift between the chip inner and outer modulation and the teeth number.

4.2 Results and discussions:

In this application we have chosen to test the methodology on two different machining systems. The chosen process is reaming operation. In the simulation two different tools are considered to be tested on the machine tool in order to estimate the critical stability limits of both. All of the tools characteristics are detailed on the Tab.1 The considered cutting pressure in this simulation is k_t(1100 MPa) for cast iron and carbide tool application. The factor k_r is equal to 0,35.

Simulations were performed on the two different combinations of the spindle and the tools, taking into account the critical depth of cut criterion to evaluate the dynamic behavior of the different systems. As shown through the Fig. 12, the critical depth of cut is 0.28 mm for the first tool against 0.18 mm for the second. Knowing that the used machine tool was the same in both similations, the gap is explained by the difference of the stiffness of the first mode of each tool. The presented approach, as shown through the depicted results in the Fig. 12, is helpful to estimate quickly the critical depth of cut for a given machining system. It can be very useful in the process design stage for estimating and comparing the critical depth of cut of different systems.This criterion as defined in this study does not take into account the axial and torsional dynamic behavior of the system. It is based on the hypothesis that chatter in reaming process is ruled by the lateral dynamic properties.

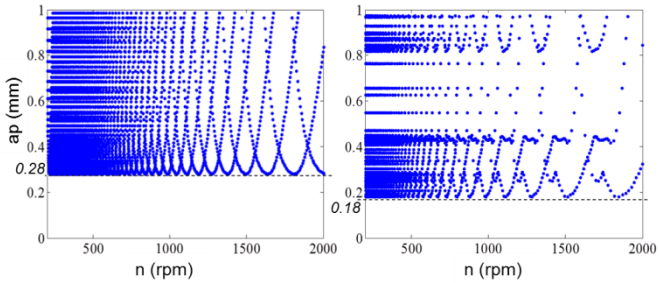

Fig. 12: Stability chart for the machining system : The spindle and the $Tool_1$ (on the left) and the spindle and the $Tool_2$ (on the right)

It was shown in the subsection (2.3) that the difference between measured and calculated FRF is small. Nevertheless, both of them represent the machining system when the tool tip is free. During machining, the dynamic properties of the tool are different since the contact and the speed of cut alter the stiffness and the damping [Jochem 2007]. Thus, this fact can have an influence on the stability limits. Moreover, at low speed, when the tooth passing period is considerably higher than the chatter vibration period, the stability becomes difficult to model because of process damping. This can be explained by the appearance of a significant number of wave left by the tool on the workpiece. It creates a variation of the clearance angle of the tool during the operation. The created waves on the surface generate a resitant force at the opposite direction of the motion. Altintas and Weck [Altintas 2004] pointed out that there is no mathematical model for representing the interaction between the tool clearance and the wavy surface.

The cutting factors k_t and k_r are a tool and material dependent quantities and are estimated for an operating point. Since the machining is made in these conditions, the linearity of the cutting law is valid and can be used for stability chart establishment. In this way, the critical depth of cut depends also on the feed rate which should be taked into account through the cutting factors.

4.3 Conclusions

In this paper a method for machining system dynamic behavior prediction at the tool tip is illustrated and compared against experimental tasks. Knowing that the chatter stability is dependent of the dynamic behavior of the machining system, the predicted functions have been used for stability chart establishment in reaming process with two different tools. Besides, the prediction FRF model was validated experimentally through hammer trials and results were accurate enough for stability lobes fitting. A dynamic model for chatter vibration in reaming process was later presented and used the predicted FRF at the reamer tips for stability lobes establishment. In summary, the presented methodology includes three main steps :

• The identification of the FRF matrix of the spindle and the tool holder by decoupling the referenc tool FRF.

• The transversal FRF at the reaming tool point is predicted by FRF coupling.

• The stability lobes are predicted and lead to the determination of the critical depth of cut ap_{cri}.

Althrough the presented method, the machine tool and the tool potentential to run a heavy reaming can be quickly evaluated and compared rapidly to other systems. It can be very helpful in the design stage of the machining process, in order to select a couple spindle and tool for a given operation. The same methodology can be applied for other machining operations as milling and drilling.

References

Paper in a journal:

[Catania 2011] G. Catania and Nicolo Mancinelli. Theoretical – experimental modeling of milling machines for the prediction of chatter vibration. International Journal of Machine Tools and Manufacture, 51(4) :339 _348, 2011.

[Erturk 2006a] A. Erturk, H.N. Ozguven, and E. Budak. Analytical modeling of spindletoo ldynamics on machine tools using timoshenko beam model and receptance coupling for the prediction of tool point {FRF}. International Journal of Machine Tools and Manufacture, 46(15) :1901 _ 1912, 2006.

[Gagnol 2011] V. Gagnol, Thien-Phu Le, and Pascal Ray. Modal identi_cation of spindle-tool unit in high-speed machining. Mechanical Systems and Signal Processing, 25(7) :2388 _ 2398, 2011.

[Gurney 1961] J-P. Gurney. A graphical method for the determination of the dynamic stability of machine tools, international journal of machine tool design and research. Benstone instruments, 1 :148_156, 1961.

[Ozsahin 2009] O. Ozsahin, A. Erturk, H.N. Ozguven, and E. Budak. A closed-form approach for identi_cation of dynamical contact parameters in spindleholder- tool assemblies. International Journal of Machine Tools and Manufacture, 49(1) :25 _ 35, 2009.

[Peklenik 1967] J. Peklenik and J.R. Gartner. Workpiece accuracy criterion for the dynamic machine tool acceptance test. International Journal of Machine Tool Design and Research, 7(4) :303 _ 324, 1967.

[Sadek 1970] M. M. Sadek and S. A. Tobias. Comparative dynamic acceptance tests for machine tools applied to horizontal milling machines. Proceedings of the Institution of Mechanical Engineers, 185(1) :319_337, 1970.

[Tobias 1962] S-A. Tobias. Dynamic acceptance tests for machine tools. International Journal of Machine Tool Design and Research, 2 :267_280, 1962.

[Tobias 1965] S.A. Tobias. Machine tool vibration. Blackies and Son, London, 1965.

[Wang 1996] J.H. Wang. Suppression of chatter vibration of a cnc machine center an exemple. Mechanical Systems and Signal Processing, 10 :551_560, 1996.

[Yuce 1983] M. Yuce. Pulse excitation technique for determining frequency response of machine tools using an on-line minicomputer and a non-contacting electromagnetic exciter. International Journal of Machine Tool Design and Research, 23 :39_51, 1983.

Paper in proceedings:

[Abele 2010] E. Abele, Y. Altintas, and C. Brecher. Machine tool spindle units.{CIRP} Annals - Manufacturing Technology, 59(2) :781 _ 802, 2010.

[Abele 2004] E. Abele and U. Fiedler. Creating stability lobe diagrams during milling.{CIRP} Annals - Manufacturing Technology, 53(1) :309 _ 312, 2004.

[Altintas 1995] Y. Altintas and E. Budak. Analytical prediction of stability lobes inmilling. CIRP Annals - Manufacturing Technology, 44 :357_362, 1995.

[Altintas 2004] Y. Altintas and M. Weck. Chatter stability of metal cutting and grinding.{CIRP} Annals - Manufacturing Technology, 53(2) :619 _ 642, 2004.

[Jochem 2007] Jochem C. Roukema and Yusuf Altintas. Generalized modeling of drilling vibrations. part ii : Chatter stability in frequency domain. International Journal of Machine Tools and Manufacture, 47(9) :1474_ 1485, 2007. Selected papers from the 2nd International Conference on High Performance Cutting 2nd {CIRP} International Conference on High Performance Cutting.

[Namazi 2007] Mehdi Namazi, Yusuf Altintas, Taro Abe, and Nimal Rajapakse. Modeling and identi_cation of tool holder - spindle interface dynamics. International Journal of Machine Tools and Manufacture, 47(9) :1333 _ 1341, 2007. Selected papers from the 2nd International Conference on High Performance Cutting 2nd {CIRP} International Conference on High Performance Cutting.

[Tlusty 1954] J. Tlusty and L.r. Spacek. Self-excited vibrations on machine tools. Publication of the Czech Academy of Sciences (Nakl. CSAV in Czech), 1954.

Technical reports or thesis:

[Erturk 2006b] A. Erturk. Dynamic modeling of spindle - tool assemblies in machining centers. PhD thesis, 2006.

[Gagnol 2006] V. Gagnol. Modelisation du comportement dynamique des electrobroches UGV. PhD thesis, 2006.

[Koppka 2008] F. Koppka, A contribution to maximization of productivity and workpiece quality of the reaming process by analyzing its static and dynamic behavior, PhD thesis, Darmstadt, December 2008

[Pruvot 1995] F. Pruvot. Conception et calcul des machines-outil. Benstone instruments, 3 :344 pages, 1995.